



Cite this: *J. Mater. Chem. C*, 2022, **10**, 3729

## Sodium doping for enhanced performance by highly efficient $\text{CsPbBr}_3$ quantum dot-based electroluminescent light-emitting diodes<sup>†</sup>

Yi Huang,<sup>a</sup> Pengfei Tang,<sup>a</sup> Wenxia Zhang,<sup>ID \*a</sup> Wensheng Yan,<sup>a</sup> Bin Liu,<sup>b</sup> Xiaosheng Tang,<sup>\*ac</sup> Zhen Wang,<sup>a</sup> Yue Peng<sup>a</sup> and Weiwei Chen<sup>ID \*a</sup>

Metal halide perovskite quantum dots (QDs) are emerging as promising materials for illumination and display applications owing to their unique optical and electronic properties. However, research into the doping of perovskite QDs with alkali metal cations for use in light-emitting diode (LED) devices is limited. Herein, a facile and convenient room-temperature method for synthesizing  $\text{Na}^+$ -ion-doped  $\text{CsPbBr}_3$  QDs is presented. Through the optimization of the  $\text{Na}^+$  doping concentration, the as-prepared  $\text{Na}^+$ -doped  $\text{CsPbBr}_3$  QDs display a higher photoluminescence quantum yield of 94.74%, faster radiative recombination rate of  $30.4 \mu\text{s}^{-1}$ , and longer lifetime of 31.2 ns than their undoped counterparts, allowing the practical realization of high-efficiency electroluminescent QD LED (QLED) devices. As a result, a maximum luminance of  $20190 \text{ cd m}^{-2}$ , a peak current efficiency of  $34.5 \text{ cd A}^{-1}$ , and an external quantum efficiency of 8.97% for as-fabricated QLEDs are obtained; all these characteristics are higher than those of the control device with undoped  $\text{CsPbBr}_3$  QDs. Experimental studies combined with auxiliary theoretical calculations indicate that the enhanced performance can be chiefly attributed to the decreased trap defect density of the perovskite upon sodium incorporation. This research indicates the immense potential of the  $\text{Na}^+$ -doped  $\text{CsPbBr}_3$  QDs to act as an emission layer for use in the next-generation illumination and display fields.

Received 16th December 2021,  
Accepted 31st January 2022

DOI: 10.1039/d1tc05997a

rsc.li/materials-c

## 1. Introduction

The component structure of all inorganic metal halide perovskite quantum dots (QDs) is  $\text{CsPbX}_3$  ( $\text{X} = \text{Cl, Br, I}$ ). Since their first successful preparation by the Kovalenko group in 2015,<sup>1</sup> the exploration of  $\text{CsPbX}_3$  ( $\text{X} = \text{Cl, Br, I}$ ) QDs has aroused great interest in researchers because of their excellent properties, such as color tunability, narrow photoluminescence (PL) spectrum, high photoluminescence quantum yield (PLQY) and long carrier lifetime, as well as their low trap state density.<sup>2–6</sup> Recently, the development and application of solution processing of halogenated perovskites has changed the traditional semiconductor production route worldwide. With their

intriguing advantages, perovskite QDs have been widely used for many applications in light-emitting diodes (QLEDs),<sup>7</sup> solar cells,<sup>8</sup> photodetectors,<sup>9</sup> resistive switching memory and other electronic devices.<sup>10</sup> In particular, through the modification of the  $\text{CsPbX}_3$  QDs and optimization of the device structure, the external quantum efficiency (EQE) of the  $\text{CsPbX}_3$ -QD-based electroluminescent (EL) LED devices has been significantly improved from the first reported value of 0.12% to 21%.<sup>11,12</sup>

Even though perovskite QDs have made great progress in QLED devices,<sup>13–16</sup> the surface defects of perovskite QDs are still the main problem hindering their further practical application. At present,  $\text{CsPbX}_3$  QDs are generally obtained *via* the hot-injection method,<sup>17</sup> ligand-assisted reprecipitation method,<sup>18</sup> ultrasonic method,<sup>19</sup> microwave-assisted method,<sup>20</sup> and template method.<sup>21</sup> For the purposes of large-scale fabrication and low cost, the ligand-assisted reprecipitation method is the recommended synthetic method. Generally, the surface ligands, such as oleic acid and oleylamine, are important for stabilizing perovskite QDs and passivating the non-radiative recombination defects. However, because of the insulating properties of these ligands,<sup>22</sup> the charge transfer ability of the QDs will be weakened,<sup>23</sup> which has adverse effects on the performance of QLED devices.

<sup>a</sup> College of Optoelectronic Engineering, Chongqing University of Post and Telecommunications, Chongqing 400065, People's Republic of China.

E-mail: zhangwx@cqupt.edu.cn, xstang@cqupt.edu.cn, chenww@cqupt.edu.cn

<sup>b</sup> School of Electronic Science and Engineering, Nanjing University, Nanjing 210093, People's Republic of China

<sup>c</sup> School of Materials Science and Engineering, Zhengzhou University, Zhengzhou 450001, People's Republic of China

<sup>†</sup> Electronic supplementary information (ESI) available: Supporting Information is available from the Wiley Online Library or from the authors. See DOI: 10.1039/d1tc05997a

To date, surface passivation technology and the metal ion doping method have been demonstrated to be effective approaches to decrease the defect states in perovskite QDs. For instance, Young-Hoon Kim and coworkers reported the effects of amine ligands with different lengths, *i.e.*, *n*-butylamine ( $C_4N_9NH_2$ ), *n*-hexylamine ( $C_6N_{13}NH_2$ ) and *n*-octylamine ( $C_8N_{17}NH_2$ ), on  $CH(NH_2)_2PbBr_3$  QDs; the results showed that the shorter ligands could greatly improve the charge injection and transportation properties of the QDs.<sup>20</sup> Bakr and coworkers adopted the shorter ligand didodecylidimethylammonium bromide (DDAB) to replace the common ligands oleic acid and oleylamine, resulting in an obvious improvement in LED efficiency.<sup>24</sup> In addition, covering the QD surface with a wide bandgap semiconductor (CdS, ZnS) also plays a key role in passivating the defects and improves the electrical properties of perovskite QDs. Unfortunately, although this method has been successfully applied to traditional II–VI or III–V semiconductor QDs,<sup>25,26</sup> it is difficult to cover  $CsPbX_3$  QDs with a wide bandgap semiconductor, because this type of QDs are ionic crystals, and the ion (metal or halogen) exchange phenomenon occurs easily. Therefore, doping metal ions into  $CsPbX_3$  QDs has become a common method to enhance the properties of QD materials. In previous reports, doping with metal ions, such as  $Ce^{3+}$ ,  $Zn^{2+}$ ,  $Cd^{2+}$ ,  $Mn^{2+}$ ,  $Sn^{2+}$ , and  $K^+$ ,<sup>27,28</sup> has been used to improve the quality of perovskite QDs and performance of QLED devices. For example, Kim and colleagues demonstrated that doping  $Ni^{2+}$  into  $CsPbBr_3$  QDs can effectively enhance their stability and PLQY.<sup>29</sup> Compared with those dealing with B-site ion doping, there are relatively few reports on A-site cation doping. For example, Hoang and coworkers introduced  $K^+$  ions into the  $CsPbBr_3$  lattice, partially replacing the position of the  $Cs^+$  ions.<sup>30</sup> By adjusting the  $K^+$ -ion-doping concentration, the PLQY of the  $CsPbBr_3$  QDs is increased to 83.2%, revealing that introducing A-site cation doping is an effective way to adjust the optical properties of  $CsPbX_3$  QDs. All these explorations demonstrated that ion-doped  $CsPbBr_3$  QDs display potential for fabricating QLED devices. However, their performance is still hovering at a relatively low level, although the doped  $CsPbBr_3$  QDs display high PL QYs and stability. For instance, the EQE of the  $Mn^{2+}$ -doped  $CsPbBr_3$ -based QLED device from the Zeng group is only 1.49%.<sup>31</sup> The Hoang group reported an EQE of 5.6% through the use of  $K^+$ -doped  $CsPbBr_3$  QDs as an emission layer.<sup>30</sup> Recently, Kim achieved an EQE of 2.4% by using  $Ni^+$ -doped  $CsPbBr_3$  perovskite QDs in a device.<sup>29</sup> These unsatisfying results encourage us to explore a feasible doping strategy to boost the efficiency of perovskite QLED devices.

In this work, we propose a facile but valid strategy for the fabrication of  $Na^+$ -ion-doped  $CsPbBr_3$  QDs. The effects of the  $Na^+$  doping on the morphology, structure, and optical properties of the QDs and the final devices are studied in detail. Compared to the pure  $CsPbBr_3$  QDs, the optimized  $Na^+$ -doped  $CsPbBr_3$  QDs display a higher PLQY of 94.74% and a longer lifetime of 31.2 ns, demonstrating that  $Na^+$  doping is beneficial to passivate defects in the  $CsPbBr_3$  QDs. The resulting QLED based on the  $Na^+$ -doped- $CsPbBr_3$  QDs exhibited a current

efficiency of  $34.5\text{ cd A}^{-1}$  and an EQE of 8.97%, which were about 2.2-fold and 1.8-fold higher, respectively, than those of the devices with undoped  $CsPbBr_3$  QD-based QLEDs. Our work suggests that  $Na^+$ -doped  $CsPbBr_3$  QDs can serve as a luminescent material in QLED applications and other optoelectronic devices.

## 2. Experimental section

### 2.1 Materials

Cesium carbonate ( $Cs_2CO_3$ , 99.9%), sodium oleate ( $NaOA$ , 98%), formamidine acetate ( $FA(Ac)$ , 99%), lead bromide ( $PbBr_2$ , 99.99%), tetra-*n*-octyl ammonium bromide (TOAB, 98%), octanoic acid (OTAc, 99%) were bought from Macklin Inc. Didodecyl dimethylammonium (DDAB, 98%) was purchased from Yuanye Corporation. Poly(3,4-ethylenedioxothiophene):poly(styrene sulfonate) (PEDOT: PSS), poly[bis(4-phenyl)(2,4,6-trimethylphenyl)amine] (PTAA), 1,3,5-tris(1-phenyl-2-benzimidazolyl)benzene (TPBi), LiF, and Al were purchased from Xi'an Polymer Light Technology Corporation. Ethyl acetate and toluene were of analytical grade and obtained from Aladdin.

### 2.2 Synthesis of $Na^+$ -doped $CsPbBr_3$ QDs

The  $Na^+$ -doped  $CsPbBr_3$  perovskite QDs were synthesized at room temperature. First, 0.1 mmol of  $Cs_2CO_3$  and  $NaOA$  were loaded into a centrifuge tube with 1 mL of OTAc. The  $Na:Cs$  proportions were controlled at 0, 1/3, 1, and 4. Subsequently, 0.2 mmol of  $FA(Ac)$  was loaded into a centrifuge tube with 1 mL of OTAc. The  $PbBr_2$  precursor solution was obtained by dissolving 1 mmol of  $PbBr_2$  and 2 mmol of TOAB in 10 mL of toluene, and the DDAB solution was obtained by dissolving 10 mg of DDAB in 1 mL toluene. Next, 0.85 mL of the cesium/sodium mixed precursor solution and 0.15 mL of the  $FA(Ac)$  solution were injected into 9 mL of the  $PbBr_2$  toluene solution. The solution was stirred and reacted for 5 min. After that, 3 mL of the DDAB solution was poured into the  $PbBr_2$  precursor solution to obtain the crude solution of  $CsPbBr_3$ . After 2 min, two equivalents of ethyl acetate were added to the  $CsPbBr_3$  crude solution, and it was centrifuged at 9000 rpm for 5 min. The precipitate was collected and redispersed in toluene. The process was repeated once more, and the precipitate was collected, redispersed in hexane and centrifuged at 4000 rpm for 5 min. Finally, the supernatant was filtered using a 0.22  $\mu\text{m}$  filter.

### 2.3 Fabrication of QLED devices

Pre-patterned ITO (South China Science Technology) glass substrates were cleaned using detergent, deionized water, acetone, and ethanol for 15 min each. After drying, the ITO substrates were treated with ultraviolet/oxygen for at least 30 min. A PEDOT:PSS solution (filtered through a 0.22  $\mu\text{m}$  filter) was spin-coated onto the ITO glass substrates at 4000 rpm for 60 s and annealed at 140 °C for 15 min. The substrates were then moved into a nitrogen glovebox. PTAA (in chlorobenzene, 8 mg  $\text{mL}^{-1}$ ) and  $CsPbBr_3$  QDs (in hexane) were deposited layer-by-layer through spin-coating at 2000 rpm for 40 s. The PTAA and QD layers were annealed at 120 °C for

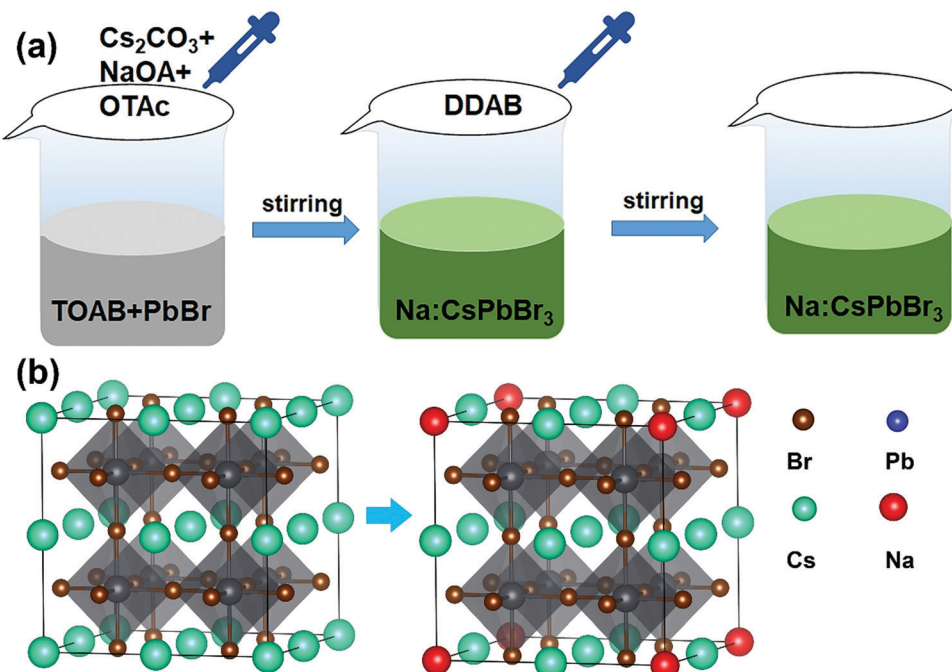


Fig. 1 (a) A schematic illustration of the synthesis procedure of  $\text{Na}^+$ -doped  $\text{CsPbBr}_3$  QDs. (b) A representative model of  $\text{Na}^+$ -doped  $\text{CsPbBr}_3$  QDs showing the replacement of some Cs positions with Na atoms.

15 min and  $60^\circ\text{C}$  for 10 min. Finally, TPBi (40 nm) and LiF/Al electrodes (1 nm/100 nm) were deposited using thermal evaporation under a high vacuum of  $2 \times 10^{-4}$  Pa. The effective area of the device is  $3\text{ mm} \times 3\text{ mm}$  square based on the overlapping area of the ITO and Al electrodes.

#### 2.4 Characterization

Transmission electron microscopy (TEM) images were recorded using a FEI Tecnai G2 F20 operated at an acceleration voltage of 200 kV. Powder X-ray diffraction (XRD) patterns were characterized using a powder diffractometer with  $\text{Cu K}\alpha$  radiation ( $= 1.5406\text{ \AA}$ ) at 36 kV and 20 mA. X-Ray photoelectron spectroscopy (XPS) analysis was carried out on a Thermo ESCALAB 250XI. The excitation source was Al Ka X-rays ( $\text{HV} = 1486.6\text{ eV}$ ) and the working voltage was 12.5 kV. The PL spectra were measured using an FLS920 spectrofluorometer. The absorption spectra were measured with a Carry 5000 spectrometer. PLQY was measured using a spectrofluorometer (JASCO, FP-8500) with an integrating sphere. Time-resolved PL measurements were collected using a fluorescence lifetime measurement system (QM/TM/NIR, PTI, America). The current density–voltage–luminance characteristics were collected using a Keithley 2450 source. The EL spectra of the devices were determined using a photo research spectra scan spectrometer PR670 in air without encapsulation.

### 3. Results and discussion

The  $\text{Na}^+$ -doped  $\text{CsPbBr}_3$  QDs with different Na/Cs ratios (0, 1/3, 1 and 4) were prepared *via* a facile room-temperature synthesis

method under ambient conditions, as shown in Fig. 1a. Different from the traditional method, in which oleic acid and oleylamine are used as ligands, here, OTAc and DDAB served as ligands, and  $\text{NaOA}$ ,  $\text{Cs}_2\text{CO}_3$  and  $\text{PbBr}_2$  provided  $\text{Na}^+$ ,  $\text{Cs}^+$ ,  $\text{Pb}^{2+}$  and  $\text{Br}^-$  for the preparation of  $\text{Na}^+$ -doped  $\text{CsPbBr}_3$  QDs. Detailed procedures for the QD fabrication are described in the Experimental Section. To elucidate the atomic coordination and occupancy parameters of the sodium ion within the cubic perovskite lattice, we performed supplementary density functional theory (DFT) calculations in which various substitution sites of sodium were considered, and adopted the Perdew–Burke–Ernzerhof (PBE) functional for the exchange–correlation interactions between the valence electrons. The force and energy convergence thresholds were set to  $-0.03\text{ eV \AA}^{-1}$  and  $10^{-6}\text{ eV}$ , respectively. For the  $2 \times 2 \times 2$  supercell calculations, we used the same convergence thresholds (cutoff energy of 300 eV). As shown in Fig. S1 in the ESI,† the formation energies for the sodium substituted on the Cs site, vacancy site, Pb site and Br site are  $-1.57\text{ eV}$ ,  $-6.66\text{ eV}$ ,  $-1.88\text{ eV}$ , and  $2.12\text{ eV}$ , respectively. The smallest formation energy appears at the sodium substituted on the Cs site. We can conclude that only when the Cs site is substituted by sodium can the perovskite cubic structure exist as the most stable state. Fig. 1b depicts a schematic illustration of a perovskite  $\text{CsPbBr}_3$  crystal after the substitution of  $\text{Cs}^+$  with smaller  $\text{Na}^+$  ions. Because the  $\text{Na}^+$  ions are smaller than  $\text{Cs}^+$ , lattice contraction emerged after the partial substitution of  $\text{Cs}^+$  ions by  $\text{Na}^+$  ions.

The XRD patterns of the  $\text{Na}^+$ -doped  $\text{CsPbBr}_3$  QDs with different Na/Cs ratios are shown in Fig. 2a. All diffraction peaks can be readily identified in the XRD patterns of the  $\text{CsPbBr}_3$

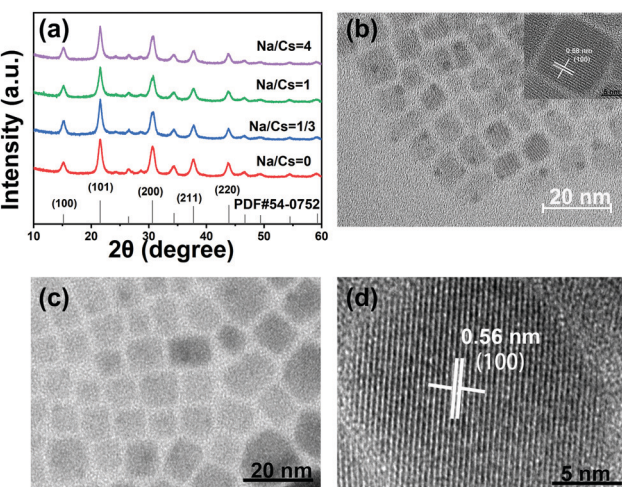


Fig. 2 (a) XRD patterns of the as-synthesized  $\text{Na}^+$ -doped  $\text{CsPbBr}_3$  QDs with different  $\text{Na}/\text{Cs}$  ratios. TEM images of (b)  $\text{CsPbBr}_3$  and (c) representative  $\text{Na}^+$ -doped  $\text{CsPbBr}_3$  QDs ( $\text{Na}/\text{Cs} = 1:3$ ). (d) A HRTEM image of a typical  $\text{Na}^+$ -doped  $\text{CsPbBr}_3$  QD. The inset of (b) shows a HRTEM image of one  $\text{CsPbBr}_3$  QD.

QDs, indicating that the crystal structure of these QDs corresponds to the cubic phase (PDF#54-0752). Additionally, it is readily observed that no impurity peaks can be found in the XRD patterns of the  $\text{Na}^+$ -doped  $\text{CsPbBr}_3$  QDs, revealing the intact crystalline nature of the QDs prepared at different doping concentrations and indicating that the  $\text{Na}^+$  doping does not affect the crystalline structure of the  $\text{CsPbBr}_3$  hosts. The morphology characterization of the undoped and doped  $\text{CsPbBr}_3$  QDs was carried out *via* TEM measurements. Fig. 2b shows that the as-prepared  $\text{CsPbBr}_3$  QDs display a cubic shape

with a uniform size. The inset of Fig. 2b is the high-resolution TEM (HRTEM) image of a single  $\text{CsPbBr}_3$  QD, which reveals that its interplanar distance of 0.58 nm is highly consistent with the (100) plane of cubic-phase  $\text{CsPbBr}_3$  QDs. Fig. 2c displays the TEM image of the as-synthesized  $\text{Na}^+$ -doped  $\text{CsPbBr}_3$  QDs ( $\text{Na}/\text{Cs} = 1/3$ ). The cubic morphology of the doped QDs is similar to that of the undoped  $\text{CsPbBr}_3$  QDs. Excellent dispersion and a uniform size distribution are also observed for the  $\text{Na}^+$ -doped QDs. The HRTEM image reveals that the as-synthesized doped QDs have clearly observable crystal lattices with an interplanar distance of 5.6 Å (Fig. 2d). The interplanar distance reduction can be ascribed to the lattice shrinkage caused by the substitution of smaller  $\text{Na}^+$  ions for larger  $\text{Cs}^+$  ions.

To further confirm that the sodium ions are introduced into the crystal lattice, a sample of  $\text{CsPbBr}_3$  and the  $\text{Na}^+$ -doped QDs ( $\text{Na}/\text{Cs} = 1/3$ ) were analyzed using XPS measurements. As shown in Fig. 3a, the XPS survey spectrum of the  $\text{Na}^+$ -doped  $\text{CsPbBr}_3$  QDs clearly depicts signals of the elements Na, Cs, Pb and Br. As expected, the small binding energy peaks at 1071.3 eV shown in Fig. 3b correspond to the  $\text{Na} 1s$  signal, which is detected only in the  $\text{Na}^+$ -doped  $\text{CsPbBr}_3$  QDs.<sup>32,33</sup> This suggests that  $\text{Na}^+$  enters the  $\text{CsPbBr}_3$  lattice and retains the  $\text{Na}^+$  state. No differences are observed for the  $\text{Cs} 3d_{3/2}$  and  $\text{Cs} 3d_{5/2}$  signals in the XPS spectra of the  $\text{Na}^+$ -doped and undoped  $\text{CsPbBr}_3$  QDs (Fig. S2, ESI†). Interestingly, compared to those of the undoped QDs, the  $\text{Pb} 4f_{5/2}$  and  $\text{Pb} 4f_{7/2}$  peaks of the  $\text{Na}^+$ -doped QDs are shifted 0.5 eV, and the  $\text{Br} 3d_{3/2}$  and  $3d_{5/2}$  peaks are shifted 0.3 eV. These results indicate changes in the chemical environment after  $\text{Na}^+$  ion doping, further demonstrating that the  $\text{Na}^+$  ions partially replace the  $\text{Cs}^+$  ionic sites through doping reactions.

Samples with different  $\text{Na}^+$  ion concentrations ( $\text{Na}/\text{Cs} = 0, 1/3, 1, 4$ ) were prepared to investigate the optical properties of

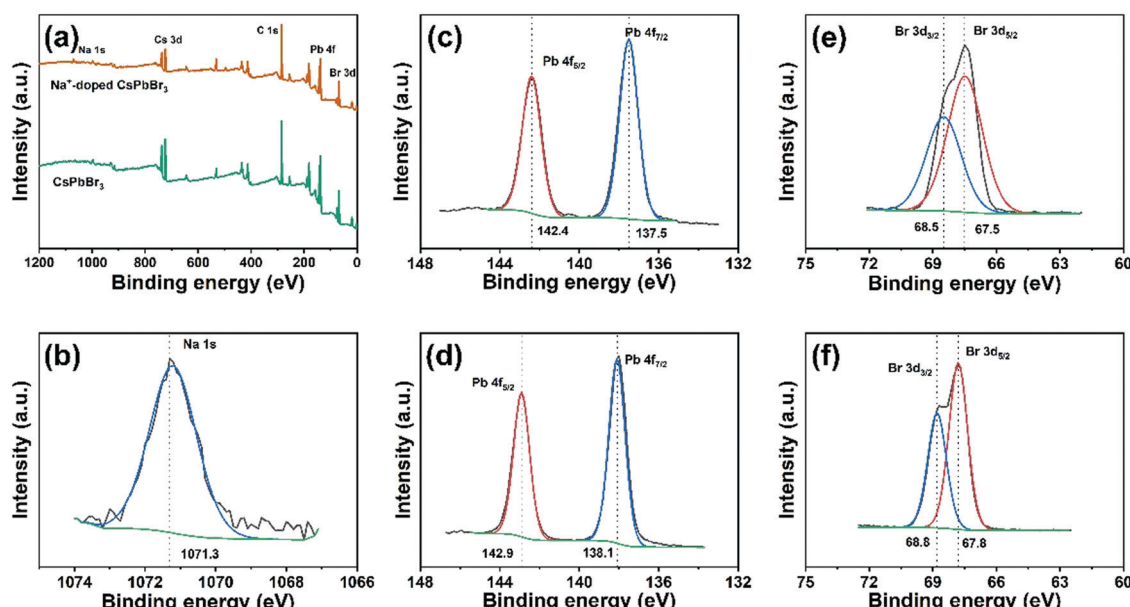


Fig. 3 (a) Survey XPS spectra of  $\text{CsPbBr}_3$  and  $\text{Na}^+$ -doped  $\text{CsPbBr}_3$  QDs ( $\text{Na}/\text{Cs} = 1/3$ ). (b) The high-resolution XPS spectrum of the  $\text{Na} 1s$  signal in the  $\text{Na}^+$ -doped  $\text{CsPbBr}_3$  QDs. (c–f) High-resolution XPS spectra corresponding to the Pb and Br elements in doped and undoped  $\text{CsPbBr}_3$  QDs. The black curves represent the original data, the blue and red curves are the fitting peaks, and the green lines are the background.

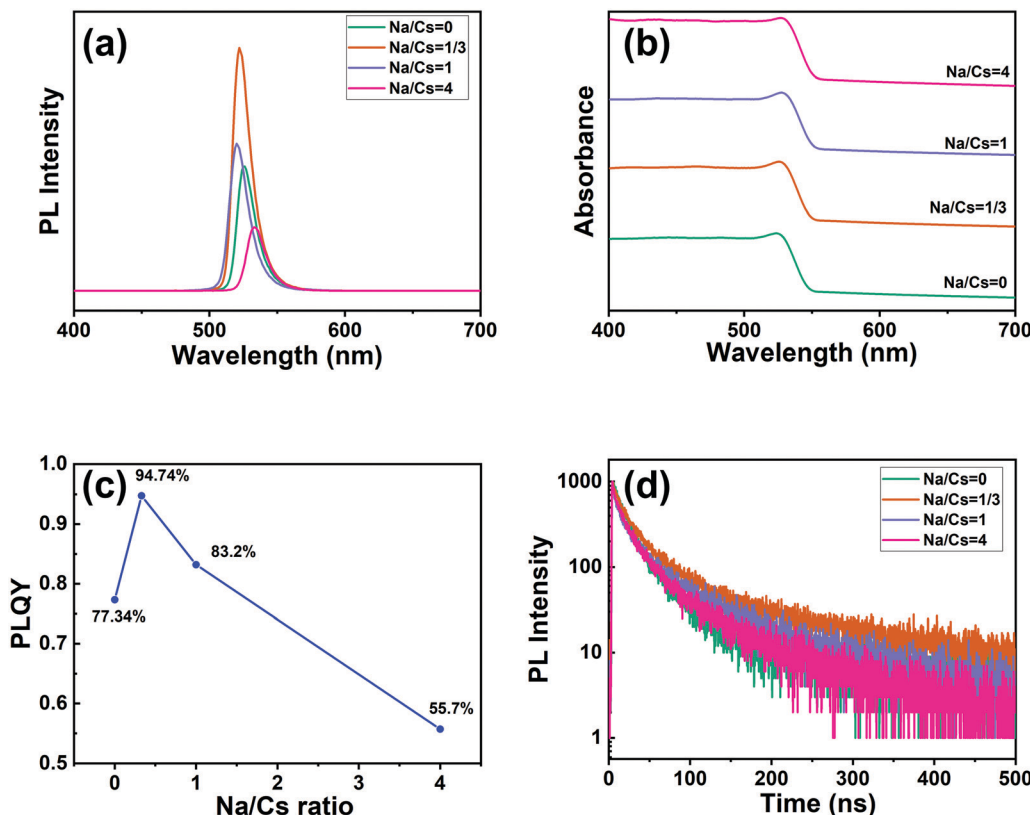


Fig. 4 (a) PL spectra (excited by 365 nm light), (b) absorption spectra, (c) PLQY data, and (d) time-resolved PL decay curves of  $\text{CsPbBr}_3$  and  $\text{Na}^+$ -doped  $\text{CsPbBr}_3$  QDs.

the  $\text{Na}^+$ -doped  $\text{CsPbBr}_3$  QDs. As shown in the PL spectra in Fig. 4a, the PL peaks are located in the range of 520–533 nm. Closer inspection reveals that the PL peaks of the  $\text{Na}^+$ -doped  $\text{CsPbBr}_3$  QDs blue-shift very slightly from 526 nm to 520 nm as the Na/Cs molar ratio is increased from 0 to 1. With further increasing the Na/Cs molar ratio to 4, the PL spectrum shifts to the right, implying that the PL is split, and the emission of the  $\text{CsPbBr}_3$  QDs dominates the spectrum. Fig. 4b shows the absorbance spectra of the  $\text{CsPbBr}_3$  QDs for the different  $\text{Na}^+$  doping concentrations. With increasing  $\text{Na}^+$  ion ratio, the absorption edges of the  $\text{Na}^+$ -doped  $\text{CsPbBr}_3$  QDs maintain almost the same energy, which indicates that the doping of  $\text{Na}^+$  ions has a slight effect on the bandgap of  $\text{CsPbBr}_3$  QDs. For a more detailed comparison of the variation in the PLQY with different sodium ion concentrations, as shown in Fig. 4c. It can be found that with increasing sodium concentration ( $\text{Na/Cs} = 0\text{--}4$ ), the PLQY first increases and then decreases. At a Na/Cs ratio of 1/3, the maximum PLQY of 94.74% was achieved, which was 1.22 times larger than that of fresh  $\text{CsPbBr}_3$  QDs. However, when the Na/Cs ratio reaches 4/1, the PLQY drops severely to 55.7%. The reason for this phenomenon can be explained as follows: excessive  $\text{Na}^+$  ions could lead to an increase in defects, thus increasing non-radiative recombination. The relevant photographs of the perovskite QDs with different doping concentrations under daylight and UV light are shown in Fig. S4 (ESI†).

Stability experiments for the doped and undoped perovskite QDs were conducted. Firstly, to evaluate the stability related to water

resistance, the sodium-ion-doped and undoped perovskite QDs were dispersed in a mixed solution of water and *n*-hexane and stirred for 90 min. Color variations for both samples were recorded. As illustrated in Fig. S5 (ESI†), the bright emission for both the undoped and doped QDs dropped with increasing storage time. However, the emission of the undoped QDs completely disappeared after 90 min of stirring, demonstrating that sodium-ion-doping could enhance the water stability of the perovskite quantum dots to some extent. We also investigated the emission of films of the doped and undoped perovskite QDs; both were annealed at 120 °C under atmospheric conditions. As shown in Fig. S6 (ESI†), when the undoped QD film was annealed for 100 min, its emission intensity was obviously decreased. The emission intensity of the doped QD film decreased only a little. Specifically, after annealing for nearly 300 minutes, the brightness of the undoped sample is significantly lower than that of the doped sample. This result proves that the doped sample shows better thermal stability than the undoped one.

The time-resolved PL decays of the  $\text{CsPbBr}_3$  QDs and  $\text{Na}^+$ -doped  $\text{CsPbBr}_3$  QDs were measured under an identical excitation wavelength of 375 nm (Fig. 4d). A tri-exponential relation can be chosen to fit the decay lifetimes of the above samples:

$$A(t) = A_1 \exp(-t/\tau_1) + A_2 \exp(-t/\tau_2) + A_3 \exp(-t/\tau_3) \quad (1)$$

Here,  $A_1$ ,  $A_2$ ,  $A_3$  and  $\tau_1$ ,  $\tau_2$ ,  $\tau_3$  are the weights and lifetime constants, respectively, of the multiple exponential functions

used for analyzing the emission lifetimes. The average lifetime ( $\tau_{\text{ave}}$ ) can be calculated by:

$$\tau_{\text{ave}} = (A_1 \tau_1^2 + A_2 \tau_2^2 + A_3 \tau_3^2) / (A_1 \tau_1 + A_2 \tau_2 + A_3 \tau_3) \quad (2)$$

The average lifetime for the excitonic luminescence of the pure  $\text{CsPbBr}_3$  QDs is 25.6 ns. It is found that the average PL decay lifetime becomes longer (31.2 ns) as the Na/Cs molar ratio is increased to 1/3. The average PL lifetime then decreases regularly with increased Na doping concentration. Concretely, the calculated result for  $\text{Na/Cs} = 1$  is 28.5 ns, and that for  $\text{Na/Cs} = 4$  is 22 ns; this reduction in PL decay indicates that the non-radiative recombination increases. The radiative and non-radiative decay rates can also be calculated using the following equations:

$$\eta_{\text{rad}} = \frac{\text{PLQY}}{\tau_{\text{ave}}} \quad (3)$$

$$\eta_{\text{non-rad}} = \frac{1 - \text{PLQY}}{\tau_{\text{ave}}} \quad (4)$$

The radiative recombination rate and non-radiative recombination rates are summarized in Table 1. It is found that the maximum radiative recombination rate reaches  $30.4 \mu\text{s}^{-1}$  for the  $\text{Na}^+$ -doped  $\text{CsPbBr}_3$  QDs with a Na/Cs ratio of 1/3. This corresponds to the shortest non-radiative recombination rate ( $1.68 \mu\text{s}^{-1}$ ). All these results suggest that  $\text{Na}^+$  ion doping can control the non-radiative recombination and promote luminescence efficiency, which directly dominates the QLED device performance.

To further clarify the roles of the  $\text{Na}^+$  ion doping in the lattice structure and luminescence efficiency, we performed related auxiliary density functional theory (DFT) calculations.

**Table 1** PLQYs, average lifetimes, radiative recombination rates, and non-radiative recombination rates of  $\text{Na}^+$ -doped  $\text{CsPbBr}_3$  QDs with different Na/Cs ratios

Na/Cs	$\tau_{\text{ave}}$ (ns)	PLQY (%)	$\eta_{\text{rad}}$ ( $\mu\text{s}^{-1}$ )	$\eta_{\text{non-rad}}$ ( $\mu\text{s}^{-1}$ )
0	25.6	77.34	30.2	8.8
1/3	31.2	94.74	30.4	1.6
1	28.5	83.2	29.2	5.9
4	22	55.7	25.3	20.1

The projected crystal orbital Hamilton population (COHP) bonding analysis shown in Fig. 5a confirms that the Na–Br bonds in cubic  $\text{CsPbBr}_3$  are slightly more stable, by *ca.* 0.23 eV, than the Cs–Br bonds, with integrated COHP values of  $-0.65$  and  $-0.42$  eV. Additionally, the Cs–Br bond length (4.20 Å) is slightly longer than the Na–Br one (4.14 Å), indicating the lattice shrinkage caused by the substitution of smaller  $\text{Na}^+$  ions for larger  $\text{Cs}^+$  ions. This conclusion is highly consistent with the experimental results from XRD and high-resolution TEM. The calculated Cs–Br band distance was slightly larger than in the experimentally determined single crystal structure of  $\text{CsPbBr}_3$  (3.67–3.79 Å), mainly because we performed the standard DFT and employed the Perdew–Burke–Ernzerhof (PBE) exchange–correlation functional, which generally underestimates the gap value and overestimates the lattice constant.<sup>34</sup> Additionally, the calculated model is based on the QD system, which also leads to differences from the single-crystal structure. As shown in Fig. 5b, the isosurfaces of the charge density of the highest occupied band and lowest unoccupied band in the  $\text{CsPbBr}_3$  and  $\text{Na}^+$ -ion-doped  $\text{CsPbBr}_3$  QDs are very different. For the pure  $\text{CsPbBr}_3$ , the lowest unoccupied band is strongly

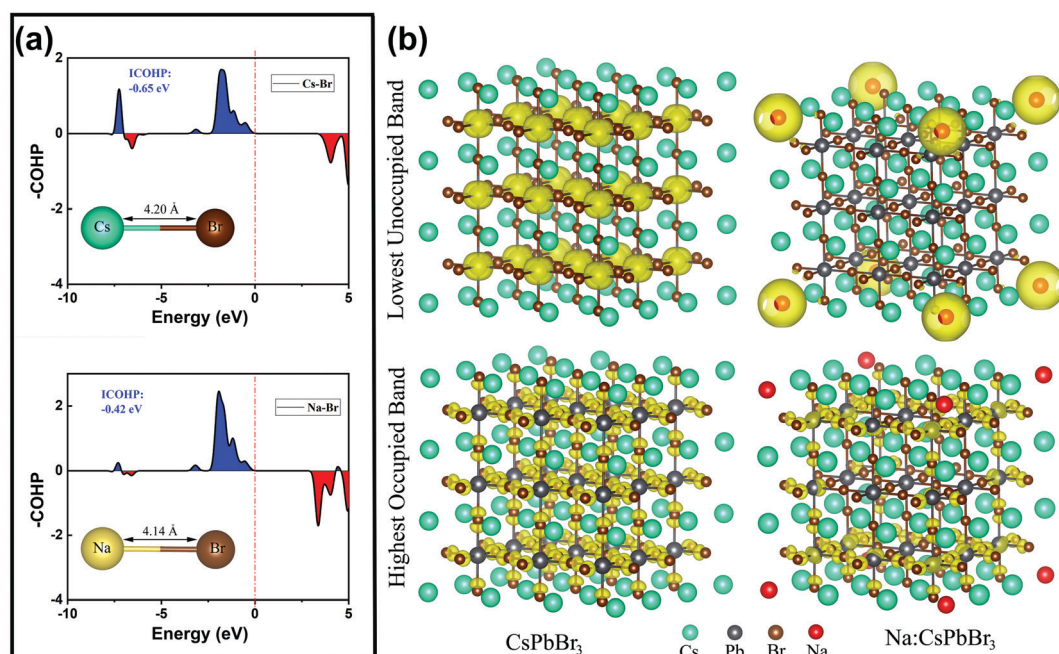


**Fig. 5** (a) COHP plots of Cs–Br and Na–Br interactions for  $\text{CsPbBr}_3$  (top) and  $\text{Na}^+$ -doped  $\text{CsPbBr}_3$  (bottom). (b) The corresponding isosurfaces of the charge density of the highest occupied band (bottom) and lowest unoccupied band (top) in  $\text{CsPbBr}_3$  and  $\text{Na}^+$ -ion-doped  $\text{CsPbBr}_3$ .

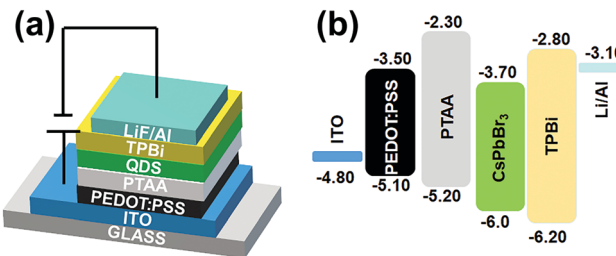


Fig. 6 (a) A schematic illustration and (b) flat-band energy level diagram of the  $\text{CsPbBr}_3$  QLED device.

localized near the  $\text{Pb}^{2+}$  ions, while for the  $\text{Na}^+$ -ion-doped  $\text{CsPbBr}_3$  QDs, it is localized around the  $\text{Na}^+$  ions, indicating that the doping of  $\text{Na}^+$  ions introduces a large number of electronic states in the lowest unoccupied orbital, leading to a reduction of defect states to some extent, which eventually induces the increase in the luminescence efficiency.

Inspired by the excellent properties of the  $\text{Na}^+$ -doped  $\text{CsPbBr}_3$  QDs with an  $\text{Na}/\text{Cs}$  ratio of 1/3, we herein employed them for the fabrication of an EL QLED device; the pure  $\text{CsPbBr}_3$  QD-based device was adopted as the control device. A schematic illustration of the optimized device is presented in Fig. 6a. The as-fabricated device is composed of multiple layers in a regular sequence as follows: ITO/PEDOT:PSS/PTAA/QDs/TPBi/LiF/Al, where the PEDOT:PSS and PTAA serve as the hole transport injection layers, and TPBi plays the role of the electron injection layer. The flat-band energy level diagram of the device is shown in Fig. 6b; the energy levels associated with all the other materials were obtained from the literature.<sup>3</sup> Fig. 7a presents the measured EL spectra of the  $\text{Na}^+$ -doped  $\text{CsPbBr}_3$  QD-based QLED device under different driving

voltages. The EL spectra peaks are located at 516 nm with a narrow full width at half maximum of 22 nm and display a high color purity in the green range. Additionally, no change in the EL spectra is observed at different driving voltages, demonstrating that the QLED device exhibits excellent spectral stability. The current density–voltage and luminance–voltage characteristics of the QLEDs based on undoped and doped  $\text{CsPbBr}_3$  QDs are shown in Fig. 7b and c, respectively. It can be noted that the difference between the current density of the doped and undoped QD devices is not large. Additionally, the turn-on voltage of 2.5 V for the  $\text{Na}^+$ -doped QD LED device is smaller than that of the control device (2.6 V) due to the enhanced electrical properties. The maximum luminance of the QLED with  $\text{Na}^+$ -doped QDs is  $20\,190\text{ cd m}^{-2}$ , which is 5.4-fold higher than that of the LED fabricated with the undoped QDs under the same carrier injection, which implies that the device based on  $\text{Na}^+$ -doped QDs has a higher electro-optic conversion efficiency. The current efficiency of the device based on the doped QDs exhibits a much higher peak value of  $34.5\text{ cd A}^{-1}$  compared to that of the control device ( $15.6\text{ cd A}^{-1}$ , Fig. 7d). Similarly, the maximum power efficiency for the  $\text{Na}^+$ -doped QD-based device is  $31.9\text{ lm W}^{-1}$  (Fig. S3, ESI†), which represents a more than 2.2-fold enhancement compared to the undoped-QD-based device. Accordingly, the best QLED device performance is achieved using the doped QDs, with a maximum EQE of 8.97% (Fig. 7e), which is a higher value than in previous reports of green QLED devices based on doped QDs. In addition, for the undoped  $\text{CsPbBr}_3$  QD-based QLED device, the luminance of the device at the peak efficiency of 4.74% is  $676.4\text{ cd m}^{-2}$ , and the EQE at the peak luminance of  $3708\text{ cd m}^{-2}$  is 1.1%. For the  $\text{Na}^+$ -doped QD-based QLED device, the luminance of the device at the peak EQE of

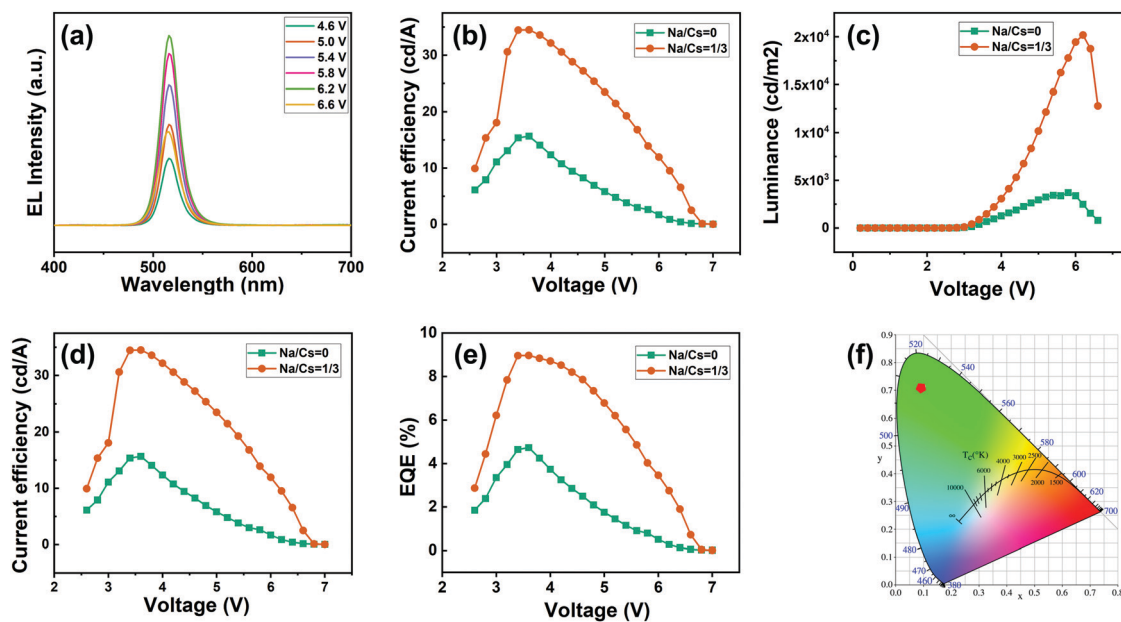


Fig. 7 (a) EL spectra of the  $\text{Na}^+$ -doped  $\text{CsPbBr}_3$  QD-based QLED device under different driving voltages. (b) Current density–voltage, (c) luminance–voltage, (d) current efficiency–voltage, and (e) EQE–voltage plots of the QLED device with undoped and  $\text{Na}^+$ -doped  $\text{CsPbBr}_3$  QDs as the emitting layer. (f) The chromaticity coordinates of the corresponding  $\text{Na}^+$ -doped  $\text{CsPbBr}_3$  QLED device.

8.97% is  $1475 \text{ cd m}^{-2}$ , and the EQE at the peak luminance of  $20190 \text{ cd m}^{-2}$  is 2.75%. These excellent results indicated the high radiative recombination and effective electrical properties of the  $\text{CsPbBr}_3$  QDs after  $\text{Na}^+$  doping. The CIE chromaticity coordinates of (0.10,0.72) are almost at the edge of the CIE chart (Fig. 7f), demonstrating the high color purity of the  $\text{Na}^+$ -doped QD-based device, and this device is thus especially suitable for wide-color-gamut display applications. The device performance is summarized in detail in Table S1 (ESI†). In addition, the performances of QLEDs based on  $\text{CsPbBr}_3$  perovskite QDs from the last six years were summarized and are shown in Table S2 in the ESI.† Although the EQE of the obtained QLED devices was not as high as that reported in other works in the literature, our work provides a new route for the development of the QLED performance.

## 4. Conclusions

In this study, we reported a simple and generalized doping strategy to obtain  $\text{Na}^+$ -doped  $\text{CsPbBr}_3$  QDs for use in high-performance QLED devices. The as-prepared  $\text{Na}^+$ -doped  $\text{CsPbBr}_3$  QDs displayed a characteristic morphology and phase structure very similar to those of their undoped counterpart, demonstrating that  $\text{Na}^+$  doping has no effect on the nucleation and growth of the  $\text{CsPbBr}_3$  QDs. Furthermore, the effects of  $\text{Na}^+$  doping on the optical and electrical properties were studied in detail. The optimized  $\text{Na}^+$ -doped  $\text{CsPbBr}_3$  QDs have a PLQY value of 94.34%, a radiative recombination rate of  $30.4 \mu\text{s}^{-1}$ , and a longer lifetime of 31.2 ns. Consequently, the QLED device based on the  $\text{Na}^+$ -doped  $\text{CsPbBr}_3$  QDs exhibited a maximum peak EQE of 8.79%, which is about 1.8-times higher than that of an undoped QD-based device. Correspondingly, the current efficiency is improved 2.2-fold from  $15.6 \text{ cd A}^{-1}$  to  $34.5 \text{ cd A}^{-1}$ . These results show that  $\text{Na}^+$  doping represents a novel method to improve the performance of perovskite QLED devices.

## Author contributions

The manuscript was written through contributions from all authors. All of the authors have given approval to the final version of the manuscript.

## Conflicts of interest

There are no conflicts of interest to declare.

## Acknowledgements

This work was supported by the National Natural Science Foundation of China (No. 62104023), Doctor Research Start-up Funding of Chongqing University of Post and Telecommunications (E012A2020018), the Technology Innovation and Application Demonstration Key Project of Chongqing Municipality [cstc2019jszx-zdztzx0005], the Science and Technology Research Program of Chongqing Municipal Education

Commission (Grant No. KJQN202100613, KJQN201900643), and Postdoctoral Project of Chongqing Science and Technology Bureau [cstc2021jcyj-bsb0250].

## References

- 1 L. Protesescu, S. Yakunin, M. I. Bodnarchuk, F. Krieg, R. Caputo, C. H. Hendon, R. X. Yang, A. Walsh and M. V. Kovalenko, *Nano Lett.*, 2015, **15**, 3692.
- 2 Y. Hassan, J. H. Park, M. L. Crawford, A. Sadhanala, J. Lee, J. C. Sadighian, E. Mosconi, R. Shivanna, E. Radicchi, M. Jeong, C. Yang, H. Choi, S. H. Park, M. H. Song, F. D. Angelis, C. Y. Wong, R. H. Friend, B. R. Lee and H. J. Snaith, *Nature*, 2021, **591**, 72.
- 3 J. Song, J. Li, L. Xu, J. Li, F. Zhang, B. Han, Q. Shan and H. Zeng, *Adv. Mater.*, 2018, **30**, 1800764.
- 4 A. Dey, J. Ye, A. De, E. Debroye, S. K. Ha, E. Bladt, A. S. Kshirsagar, Z. Wang, J. Yin, Y. Wang, L. N. Quan, F. Yan, M. Gao, X. Li, J. Shamsi, T. Debnath, M. Cao, M. A. Scheel, S. Kumar, J. A. Steele, M. Gerhard, L. Chouhan, K. Xu, X. Wu, Y. Li, Y. Zhang, A. Dutta, C. Han, I. Vincon, A. L. Rogach, A. Nag, A. Samanta, B. A. Korgel, C. Shih, D. R. Gamelin, D. H. Son, H. Zeng, H. Zhong, H. Sun, H. V. Demir, I. G. Scheblykin, I. Mora-Seró, J. K. Stolarczyk, J. Z. Zhang, J. Feldmann, J. Hofkens, J. M. Luther, J. Pérez-Prieto, L. Li, L. Manna, M. I. Bodnarchuk, M. V. Kovalenko, M. B. J. Roeffaers, N. Pradhan, O. F. Mohammed, O. M. Bakr, P. Yang, P. Müller-Buschbaum, P. V. Kamat, Q. Bao, Q. Zhang, R. Krahne, R. E. Galian, S. D. Stranks, S. Bals, V. Biju, W. A. Tisdale, Y. Yan, R. L. Z. Hoyer and L. Polavarapu, *ACS Nano*, 2021, **15**, 10775.
- 5 J. Yao, J. Wang, J. Yang and H. Yao, *Acc. Chem. Res.*, 2021, **54**, 441–451.
- 6 J. Yao, J. Ge, K. Wang, G. Zhang, B. Zhu, C. Chen, Q. Zhang, Y. Luo, S. Yu and H. Yao, *J. Am. Chem. Soc.*, 2019, **141**, 2069–2079.
- 7 D. Lee, Y. Shin, H. J. Jang, J. Lee, K. Park, W. Lee, S. Yoo, J. Y. Lee, D. Kim, J. Lee and N. Park, *ACS Energy Lett.*, 2021, **6**, 1821.
- 8 A. Swarnkar, A. R. Marshall, E. M. Sanehira, B. D. Chernomordik, D. T. Moore, J. A. Christians, T. Chakrabarti and J. M. Luther, *Science*, 2016, **354**, 92.
- 9 Y. He, M. Petryk, Z. Liu, D. G. Chica, I. Hadar, C. Leak, W. Ke, I. Spanopoulos, W. Lin, D. Y. Chung, B. W. Wessels, Z. He and M. G. Kanatzidis, *Nat. Photonics*, 2021, **15**, 36.
- 10 H. Mao, C. Gu, S. Yan, Q. Xin, S. Cheng, P. Tan, X. Wang, F. Xiu, X. Liu, J. Liu, W. Huang and L. Sun, *Adv. Electron. Mater.*, 2020, **6**, 1900493.
- 11 T. Fang, T. Wang, X. Li, Y. Dong, S. Bai and J. Song, *Sci. Bull.*, 2020, **66**, 36.
- 12 M. Liu, Q. Wan, H. Wang, F. Carulli, X. Sun, W. Zheng, L. Kong, Q. Zhang, C. Zhang, Q. Zhang, S. Brovelli and L. Li, *Nat. Photonics*, 2021, **15**, 379.
- 13 J. Zito and I. Infante, *Acc. Chem. Res.*, 2021, **54**, 1554.

14 J. Yang, Y. Song, J. Yao, K. Wang, J. Wang, B. Zhu, M. Yao, S. U. Rahman, Y. Lan, F. Fan and H. Yao, *J. Am. Chem. Soc.*, 2020, **142**, 2956–2967.

15 B. Han, S. Yuan, B. Cai, J. Song, W. Liu, F. Zhang, T. Fang, C. Wei and H. Zeng, *Adv. Funct. Mater.*, 2021, **31**, 2011003.

16 Y. Xu, Y. Cui, H. Yao, T. Zhang, J. Zhang, L. Ma, J. Wang, Z. Wei and J. Hou, *Adv. Mater.*, 2021, **33**, 2101090.

17 Q. Xiong, S. Huang, J. Du, X. Tang, F. Zeng, Z. Liu, Z. Zhang, T. Shi, J. Yang, D. Wu, H. Lin, Z. Luo and Y. Leng, *Adv. Opt. Mater.*, 2020, **8**, 2000977.

18 L. Schmidt, A. Pertegas, S. Gonzalez-Carrero, O. Malinkiewicz, S. Agouram, G. M. Espallargas, H. J. Bolink, R. E. Galian and J. Perez-Prieto, *J. Am. Chem. Soc.*, 2014, **136**, 850.

19 H. Huang, Q. Xue, B. Chen, Y. Xiong, J. Schneider, C. Zhi, H. Zhong and A. L. Rogach, *Angew. Chem., Int. Ed.*, 2017, **5**, 10947.

20 Q. Pan, H. Hu, Y. Zou, M. Chen, L. Wu, D. Yang, X. Yuan, J. Fan, B. Sun and Q. Zhang, *J. Mater. Chem. C*, 2017, **5**, 10947.

21 H. He, Y. Cui, B. Li, B. Wang, C. Jin, J. Yu, L. Yao, Y. Yu, B. Chen and G. Qian, *Adv. Mater.*, 2019, **31**, 1806897.

22 J. Li, L. Xu, T. Wang, J. Song, J. Chen, J. Xue, Y. Dong, B. Cai, Q. Shan, B. Han and H. Zeng, *Adv. Mater.*, 2017, **29**, 1603885.

23 Y. H. Kim, G. H. Lee, Y. T. Kim, C. Wolf, H. J. Yun, W. Kwon, C. G. Park and T. W. Lee, *Nano Energy*, 2017, **38**, 51.

24 J. Pan, L. N. Quan, Y. Zhao, W. Peng, B. Murali, S. P. Sarmah, M. Yuan, L. Sinatra, N. M. Alyami, J. Liu, E. Yassitepe, Z. Yang, O. Voznyy, R. Comin, M. N. Hedhili, O. F. Mohammed, Z. H. Lu, D. H. Kim, E. H. Sargent and O. M. Bakr, *Adv. Mater.*, 2016, **28**, 8718.

25 Z. Hu, S. Liu, H. Qin, J. Zhou and X. Peng, *J. Am. Chem. Soc.*, 2020, **142**, 4254.

26 Y. Wang, C. Pu, H. Lei, H. Qin and X. Peng, *J. Am. Chem. Soc.*, 2019, **141**, 17617.

27 Y. Chen, Y. Liu and M. Hong, *Nanoscale*, 2020, **12**, 12228.

28 J. Yao, J. Ge, B. Han, K. Wang, H. Yao, H. Yu, J. Li, B. Zhu, J. Song, C. Chen, Q. Zhang, H. Zeng, Y. Luo and S. Yu, *J. Am. Chem. Soc.*, 2018, **140**, 3626–3634.

29 H. Kim, S. Bae, T. H. Lee, H. Lee, H. Kang, S. Park, H. W. Jang and S. Y. Kim, *Adv. Funct. Mater.*, 2021, **31**, 2102770.

30 M. T. Hoang, A. S. Pannu, C. Tang, Y. Yang, N. D. Pham, K. Gui, X. Wang, S. Yambem, P. Sonar, A. Du and H. Wang, *Adv. Opt. Mater.*, 2020, **8**, 2000742.

31 S. Zou, Y. Liu, J. Li, C. Liu, R. Feng, F. Jiang, Y. Li, J. Song, H. Zeng, M. Hong and X. Chen, *J. Am. Chem. Soc.*, 2017, **139**, 11443.

32 Y. Ji, M. Wan, Z. Yang, H. Qiu, S. Ji, J. Dou and N. V. Gaponenko, *Nanoscale*, 2020, **12**, 6403–6410.

33 S. Li, Z. Shi, F. Zhang, L. Wang, Z. Ma, D. Yang, Z. Yao, D. Wu, T. Xu, Y. Tian, Y. Zhang, C. Shan and X. Li, *Chem. Mater.*, 2019, **31**, 3917–3928.

34 W. Kohn and L. J. Sham, *Phys. Rev.*, 1965, **140**, 1133–1138.